Prototyping of Meso- and Microfluidic Devices with Embedded TiO_2 Photocatalyst for Photodegradation of an Organic Dye

Druval S. De Sá[1], Bojan A. Marinkovic[2], Eric C. Romani[3], Tommaso Del Rosso[3], Rodrigo O. M. A. de Souza[4], Alessandro Massi[5] and Omar Pandoli[1]*

[1]*Chemistry Department, Pontificia Universidade Católica, PUC-Rio, Rio de Janeiro, 22451-900, Brazil*
[2]*Department of Chemical and Materials Engeneering, Pontificia Universidade Católica, PUC-Rio, Rio de Janeiro, 22451-900, Brazil*
[3]*Physics Department, Pontificia Universidade Católica, PUC-Rio, Rio de Janeiro, 22451-900, Brazil*
[4]*Biocatalysis and Organic Synthesis Group, Organic Chemistry Department, Chemistry Institute, Universidade Federal do Rio de Janeiro, UFRJ, Rio de Janeiro, 22451-900, Brazil*
[5]*Department of Chemistry Universitá di Ferrara, UNIFE, Ferrara, Italy*

Received: 04 November 2015; accepted: 02 May 2016

We present prototyping of meso- and microfluidic photocatalytic devices, functionalized through incorporation of TiO_2 nanoparticles in polydimethylsiloxane (PDMS), and comparison of their efficiencies for the degradation of rhodamine B (10^{-5} mol/L). The prototyping of the photocatalytic devices involves simple and low-cost procedures, which includes microchannels fabrication on PDMS, deposition and impregnation of TiO_2 on PDMS, and, finally, plugging on the individual parts. For the microfluidic device with 13 μL internal volume, photocatalytic TiO_2–PDMS composite was sealed by another PDMS component activated by O_2 plasma (PDMS–TiO_2–PDMS). For the mesofluidic device, a homemade polyetheretherketone (PEEK) flow cell with 800 μL internal volume was screwed on a steel support with a glass slide and the photocatalytic composite. The photocatalytic activities of the devices were evaluated using two different pumping flow systems: a peristaltic pump and a syringe pump, both at 0.05 mL/min under the action of 365 nm ultraviolet (UV) light. The characterization of TiO_2–PDMS composite was performed by confocal Raman microscopy, scanning electron microscopy (SEM), and energy dispersive spectroscopy (EDS). The photocatalytic microreactor was the most efficient, showing high organic dye photodegradation (88.4% at 12.5 mW/cm^2).

Keywords: flow reactor, photocatalysis, rhodamine B, composite, confocal Raman microscopy

1. Introduction

Batch reactors in heterogeneous photocatalysis have been widely used; however, the need to improve these systems has awakened interest in micro- and mesoreactors continuous-flow technology [1–3]. The continuous-flow regime has several advantages in comparison to traditional batch reactors: more efficient control of reaction parameters, efficient mixing of reagents, lower cost in the optimization of the reaction conditions, and the possible utilization of online tools for reaction monitoring [4–6].

Microreactor technology (MRT) is focused on engineered manipulation of fluids in channels with micrometric dimensions, in which the laminar flow is prevalent [3]. This technology is characterized by presenting an array of channels with different geometries or volume with high capacity to control operational reaction parameters (P, V, T, concentration) and higher efficiency in heat exchange and reagents mixing [7, 8]. These systems have the potential to screen many continuous processing reaction conditions and to establish ideal conditions in small volume and reduced time [4, 9, 10].

The difference between a micro- and mesoreactor is the volumetric capacity generated from the dimensions of the channels [11]. Microreactors have channels with hydraulic diameter (DH) between 1 μm and 100 μm, while mesoreactors have DH channels between 100 μm and 1 mm [8]. Several micro- and mesofluidic systems were developed and characterized [12–15], such as medical diagnostic devices with integrated biosensors [16], circulating tumor cell capture systems [17], gradient concentration generators [18], photocatalytic water purification [19], and organic and inorganic synthetic flow reactors [9]. Despite good results, the main disadvantage of small-scale reactors is the relatively high cost combined with the low output of a single reactor and the unfeasibility of production on a commercial scale [20]. Nevertheless, a continuous-flow reactor can be numbered-up without further testing for a large-scale production; another alternative is scaling-up the volume of the flow reactor system with a mesoreactor device for industrial application [21].

The meso- and microfluidic systems can be manufactured from various materials [22], including glass, polydimethylsiloxane (PDMS), steel, and silicon [23–26]. PDMS is the most suitable for rapid prototyping of such systems being inexpensive and exhibiting a combination of important properties such as flexibility, biocompatibility, ultraviolet–visible (UV–vis) transparency, heat resistance, and chemical inertness [27–31]. The incompatibility of the PDMS with some organic solvents such as ethanol, toluene, and dichloromethane due to swelling of the polymer, restricts the use of these manufactured devices [32]. While PDMS devices cannot operate on high pressures and temperatures, on the other hand, a meso flow cell with resistant material and stable connectors can support higher flow rate and stronger chemical and temperature conditions.

The implementation in flow reactor of heterogeneous photocatalyst has been extensively studied due to its high power of degradation by oxidizing a large number of organic and inorganic compounds [33]. The main advantages of immobilization of the catalyst compared to a homogeneous system are: (1) easy isolation of the catalyst from reaction medium minimizing environmental impact, (2) the possibility of using the fixed catalysts in continuous-flow reactors, and (3) the recycling of the catalyst minimizing the cost of the reaction process [34]. The use of TiO_2 immobilized on different surfaces has increased in several research areas and in industrial applications, such as: self-cleaning surface [35], fabric treatment [36], water-repellent

* Author for correspondence: omarpandoli@puc-rio.br

DOI: 10.1556/1846.2015.00043

First published online: 8 June 2016

surface [37], water treatment [38], and catalysis [39]. The main benefits of this composite material are chemical stability, biocompatibility, commercial availability, low cost, and the active optical capacity.

Figure 1 and Eqs. 1–5 show the photocatalytic mechanism on TiO_2 surface, where TiO_2^* is the excited state of titania, OH^-_{ads} is absorbed hydroxide ions, e^-_{CB} is the photoexcited electron in the conduction band (CB), while h^+_{VB} is the electronic hole generated in the valence band (VB), $OH^\bullet$ and O_2^- are highly oxidative active species, which can significantly contribute to the photocatalytic decomposition of dye [41].

$$TiO_2 + h(UV) \rightarrow TiO_2^*\left(h^+_{VB} + e^-_{CB}\right) \quad (1)$$

$$e^-_{CB} + O_{2ads} \rightarrow O_2^- \quad (2)$$

$$H_2O_{ads} + h^+_{VB} \rightarrow H^+_{ads} + OH^\bullet \quad (3)$$

$$h^+_{VB} + OH^-_{ads} \rightarrow OH^\bullet \quad (4)$$

$$\text{dye} + OH^\bullet + O_2^- \rightarrow \text{products} \quad (5)$$

There are several techniques for prototyping photocatalytic meso- and microfluidic devices [22, 25] and various methods to integrate TiO_2 into flow reactors systems, such as chemical vapor deposition on pyrex [41], drop casting on PDMS [40], electrospun nanofibrous TiO_2 on glass [42], calcination [43] on glass, coating on fiber glass [44], and adhesive substrate [45]. These techniques should be rapid, simple, avoiding the use of a clean room with expensive photolithography techniques, and should have a low cost from the design stage to the final test. The use of TiO_2 as heterogeneous catalysis is highly effective for the selective oxidation of organic molecules and organic pollutants soluble in water, avoiding the recovery requirements for the photocatalyst present in the reaction mixture, such as in the case of a batch reactor [46–49]. Another important feature of this approach, using PDMS as the support, is to eliminate a critical step of calcinations of the TiO_2 into glass, reducing a high energy cost of prototyping and coarsening of nanocrystals. Recently, Lamberti [50] incorporated TiO_2 nanoparticles directly on the surface of PDMS to build a photocatalytic device constituted completely by PDMS. Differently to Pandoli et al. [40], who built a photocatalytic device PDMS–TiO_2–glass, this author used a PDMS–TiO_2–PDMS reactor to study the photodegradation of a methylene blue solution (6×10^{-5} mol/L) with a high intensity UV light powered at 60 mW/cm^2.

In this work, we propose a rapid and low-cost construction of meso- and microfluidic devices with embedded TiO_2 photocatalyst on PDMS for the photodegradation of rhodamine B, more stable than methylene blue as shown on our previous work [40]. In order to evaluate and compare the photocatalytic efficiency in both devices, we used as the test model the photodegradation of rhodamine B dye solution (10^{-5} mol/L), applying different UV LED light power, 25 and 12.5 mW/cm^2. Changing the UV light power, photolysis and photocatalysis contributions to the dye degradation can be distinguished. We demonstrate as a microreactor devise shows a higher efficiency of the photocatalyst embedded into a PDMS compared to the photocatalytic mesoreactor.

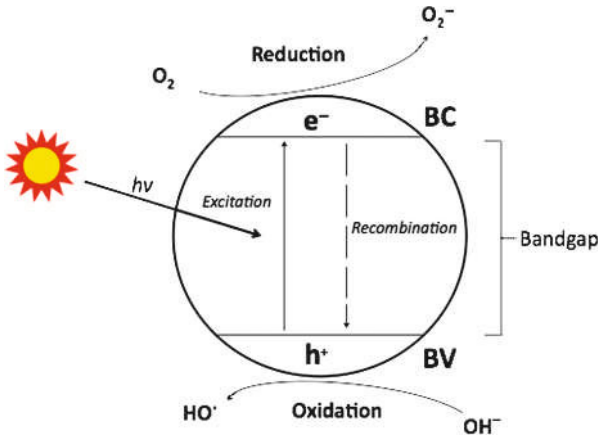

Figure 1. Photocatalytic process on TiO_2 surface

2. Results and Discussion

2.1. Characterization of PDMS–TiO_2. The impregnation of the photocatalyst into PDMS is an important step at prototyping process of photocatalytic meso- and microreactors. The photocatalyst layer needs a good adhesion on the PDMS support to avoid abrasion during the flow injection of the dye solution. The scanning electron microscopy (SEM) image shows a cross section of the PDMS–TiO_2 composite with a protrusion of ≈124 μm corresponding to the depth of the cavity where the TiO_2 suspension (1% w/v) was deposited and covered with PDMS (Figure 2). Energy dispersive spectroscopy (EDS) spectrum, inset in Figure 2, confirmed the immobilization of TiO_2 on the protrusion surface of the PDMS as indicated by the presence of Ti together with Si, while only Si was detected on the inner part of the PDMS. The presence of Ni revealed on EDS spectra is due to the use of stainless steel knife to cut the PDMS–TiO_2 composite.

The optical image of the confocal Raman microscope shows a heterogeneous mixture of TiO_2 and PDMS components (Figure 3). Colored 2D and 3D images were generated by integrating area over the intensity peak of two defined Raman spectral bands, from 133 to 143/cm for TiO_2, and from 695 to 710/cm for PDMS, showing the spatial distribution of both components. Raman 2D mapping (25 × 25 μm) overlapped above the optical image shows two areas colored in blue and green, corresponding to two components of the composite, TiO_2 and PDMS, respectively.

In Figure 4, on the top left side, the blue Raman spectrum showed an intense band at 140/cm, and other minor bands, being assigned to anatase [51]. On the bottom right side, the green Raman spectrum shows a symmetric stretching of Si–O–Si band at 490/cm and symmetric and asymmetric stretching of Si–C at 702/cm and 720/cm of pure PDMS. Raman 3D mapping allowed a visualization of a volume of 20 × 20 × 10 μm, where the blue color represents TiO_2 in the anatase form and the green area is due to PDMS-rich region (Figure 4). The 3D imaging processing shows the interface between the two components in 10 μm depth, confirming the lack of a total coverage of the photocatalytic surface.

2.2. Study of Photocatalytic Activity. Photocatalytic activity's results are presented in Figure 5, where photodegradation activity of the microreactor (after each cycle) and mesoreactor (after 16 h) is compared using two power UV LED light sources (25 mW/cm^2 and 12.5 mW/cm^2) and two different injection systems. All the values, except the data with UV LED powered at 25 mW/cm^2, are reported in Tables 1 and 2. The photodegradation process was monitored observing the absorbance change at 556 nm wavelength of the rhodamine B solution, and the percentage degradation (D%) was determined through the following equation:

$$D\% = \frac{[A_0 - A_x]}{(A_0)} \times 100 \quad (6)$$

where A_0 is the absorbance of the mother solution and A_x is the absorbance after photodegradation after some period of time. With a syringe pump system, the absorption band of rhodamine

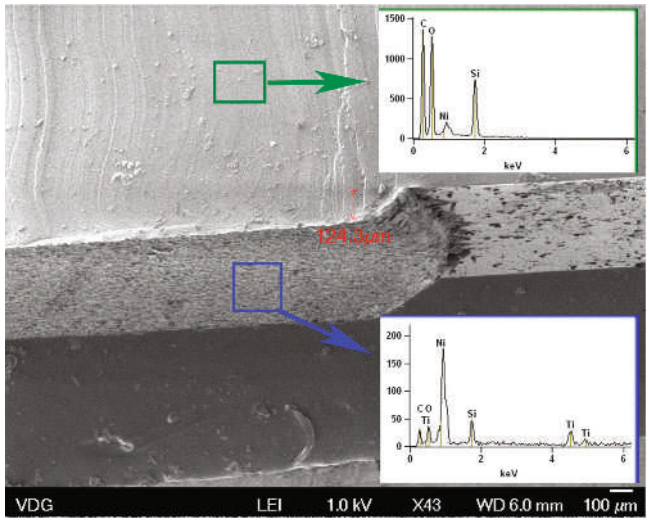

Figure 2. A SEM image and EDS spectra of a cross section of the PDMS–TiO_2 composite. In the top inset, EDS spectrum of an area outlined in green shows only the presence of Si without Ti; in the bottom inset, EDS spectrum of an area outlined in blue shows both the presence of Si and Ti

B was registered after every flow injection cycle (Figure 6A). In case of peristaltic pump loop system, the monitoring was done after 9 and 16 h (Figure 6B).

According to the histogram in Figure 5, the mesoreactor and the syringe pump system with a UV LED powered at 25 mW/cm^2 showed a discoloration of rhodamine B solution of 88.4%, while the control reached a 63.5%.

The percentage difference between the two was of ≈25% corresponding to photocatalytic degradation. A peristaltic pump with the same UV light powered at 25 mW/cm^2 showed a discoloration of rhodamine B solution of 80.5%; however, the control reached 44.8% with a percentage difference of 35.7% due to photocatalysis. The high photodegradation activity of the light itself was reduced decreasing the intensity of the UV LED power from 25 to 12.5 mW/cm^2. In this case, the action of the photolysis process was, as expected, less evident compared with the photocatalysis phenomena.

As reported in Table 1, the reduction of UV LED power to 12.5 mW/cm^2 caused the decrease of photolysis up to 18.4% with a syringe pump mesoreactor system (control), while the photocatalytic mesoreactor system reached 51.5% of photodegradation, confirming a significant difference between photocatalysis and photolysis. This means that photocatalyst layer needs only a minimum amount of UV–vis light to be activated and generate the radicals •OH_{ads} and O_2^-, consequently degrade the rhodamine B solution. Higher UV LED light intensity can increase the photolysis phenomena covering the efficiency of TiO_2. For this reason, the photocatalytic microreactor system was used only with a UV LED powered at 12.5 mW/cm^2. With double power intensity UV light, the photolysis phenomena covered the photocatalytic process. In this case, the photocatalytic microreactor with a syringe pump system at 12.5 mW/cm^2 showed 88.4% of degradation of rhodamine B solution, while the control reached 20.6% with a percentage difference of 67.8%. The microreactor system showed a performance of ≈37% higher than a mesoreactor.

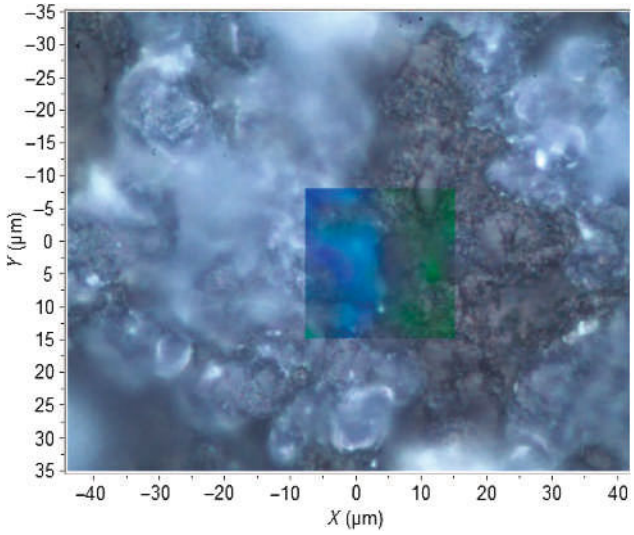

Figure 3. Optical microscopy image overlapped by colored Raman 2D spectra generated by integrating the intensities of Raman spectral bands from 133 to 143/cm for TiO_2 (blue) and from 695 to 710/cm for PDMS (green)

In peristaltic pump system (Table 2), after 16 h with 0.05 mL/min flow rate and UV LED light source of 12.5 mW/cm^2, it was found that the efficiency of the photocatalytic microreactor is two-fold higher with respect to the mesoreactor. While photocatalytic mesoreactor device showed 43.6% of discoloration, compared to 19.2% of the control, the photocatalytic microreactor presented 86.1% of discoloration, compared with the control 25.6%.

The better performance can be justified by the higher photocatalytic surface to internal volume of reactor ratio. It is important to highlight that only a small volume allows better exploration of UV light providing the formation of radicals species $OH^{\bullet}_{ads}$ and O_2^- responsible for the degradation of organic compounds [6, 43, 44] and consequently increase the photocatalytic efficiency of the microfluidic device in respect with the mesoreactor. Fixing the flow rate at 50 μL/min, the micro and meso flow cell present two different resident times (R_{Time}= volume cell/flow rate): 0.2 min and 16 min, respectively. Although the microreactor (13 μL internal volume) has a lower resident time (0.2 min), the efficiency is higher compared to the mesoreactor (800 μL internal volume) with higher resident time (16 min). This is understandable in the light of the higher intimate contact between the organic dye and the photocatalytic surface in the microreactor, while the resident time was not capable to impose its effect on the final results. Moreover, the difference between micro- and meso fluidic devices is not just the internal volume and hydraulic diameter, since velocity changes, as well. The calculation of the Reynolds number of 0.126 and 0.087, for micro- and mesoreactor, respectively, presented in detail in the supporting information, showed that low flow rate 50 μL/min, used for the photodegradation test, does not change the regime of laminar flow inside both flow cells.

Another important factor to consider is the maintenance of the catalytic activity of TiO_2–PDMS composite during repeated

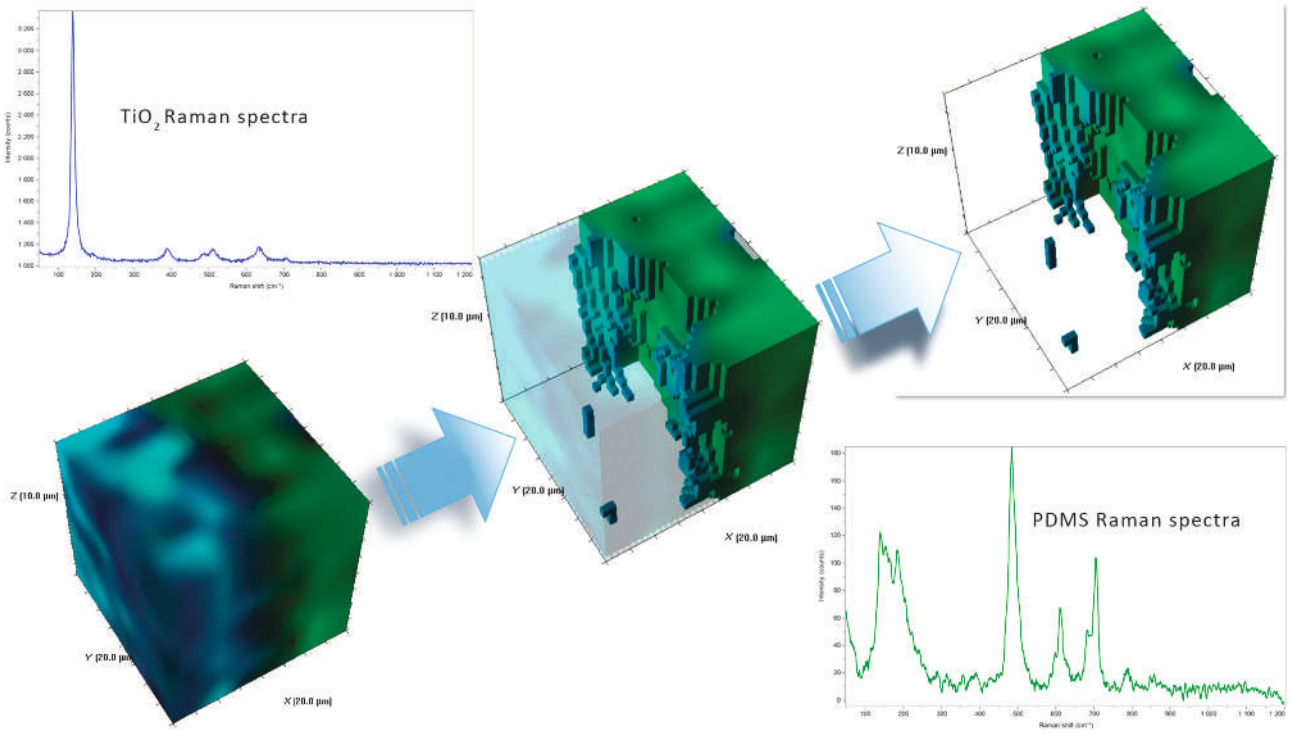

Figure 4. 3D mapping (20 × 20 × 10 μm) with confocal Raman microscopy generated by integrating the intensity of defined Raman spectral bands from 133 to 143/cm of TiO_2 (blue) and from 695 to 710/cm for PDMS (green)

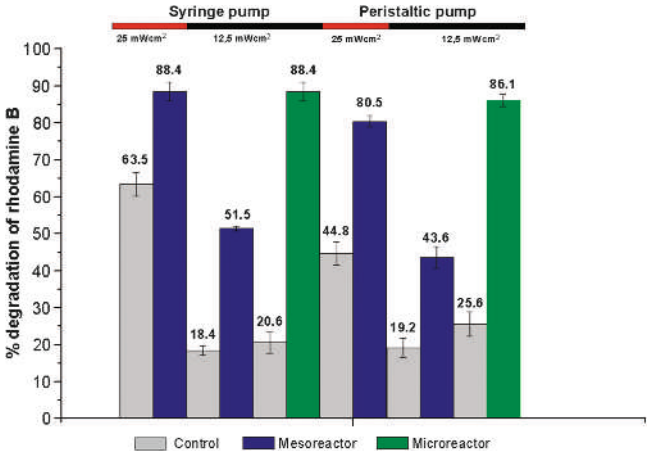

Figure 5. Photodegradation of rhodamine B solution in meso- and microreactor systems, using different pumps and UV LED powers. All solutions were injected at 0.05 mL/min flow rate

uses. In Figure S5, it is showed that the photocatalytic composite demonstrated a reduction of about 10% for microreactor and 4% for mesoreactor after the repetition of the test for 4 times in both reactors.

It is relevant to notice that the mesoreactor was also tested at higher flow rates, such as 0.1 and 0.2 mL/min, and that abrasion of the photocatalyst was not observed. This factor further reinforces the importance of proper integration of P25 in PDMS to extend the photocatalytic durability, without generation of inorganic waste.

The semicontinuous-flow system with syringe pump was useful to determine the photodegradation of rhodamine B at each step without mixing the products generated along the photocatalytic process. All values of photodegradation tests of rhodamine B in meso and microfluidic devices with syringe pump after 5 cycles at 0.05 mL/min (UV LED light source of 12.5 mW/cm^2, Table 1) were used to plot C_t/C_0 versus time dependence (Figure 7), wherein C_0 is the initial concentration of rhodamine and C_t is the concentration solution after every flow injection cycle. The photodegradation values with a meso- and microreactor system without photocatalyst (control) were plotted as references to highlight the photolysis phenomena during the UV light exposition. It is noticed that the decrease of rhodamine B concentration during the photocatalytic degradation process in the microreactor system is more pronounced than in the mesoreactor system.

The photodegradation in micro- and mesoreactor without the TiO_2 is low, which confirms photocatalytic efficiency of TiO_2 (anatase) and its good adhesion to PDMS. It is also possible to

Table 1. Photodegradation tests of rhodamine B solution 10^{-5} mol/L in meso- and microfluidic devices with syringe pump after 5 cycles at 0.05 mL/min (UV LED light source of 12.5 mW/cm^2)

Syringe pump (5 cycles)	Photodegradation (D%) of rhodamine B							
	Control	Meso I	Meso II	Meso III	Control	Micro I	Micro II	Micro III
Cycle 1	7.1	14.3	22.4	17.5	8.8	41.9	46.0	39.2
Cycle 2	10.7	25.4	29.2	28.2	12.6	54.9	61.9	58.7
Cycle 3	12.8	36.2	39.2	35.0	16.2	73.8	74.1	72.2
Cycle 4	14.3	44.8	46.0	41.6	18.0	84.7	82.2	81.3
Cycle 5	18.5	51.4	52.2	50.8	20.6	91.3	87.2	86.8
Average (%)			51.5				88.4	

The experiments were performed in triplicate with a fresh PDMS–TiO_2 photocatalytic composite named meso and micro I, II and III. For the control tests, the average values of the triplicate are indicated.

Table 2. Photodegradation test of rhodamine B solution 10^{-5} mol/L, both in meso- and microfluidic devices, with peristaltic pump after 16 h at 0.05 mL/min (UV LED light source of 12.5 mW/cm^2)

Peristaltic pump	Photodegradation (D%) of rhodamine B							
	Control	Meso I	Meso II	Meso III	Control	Micro I	Micro II	Micro III
16 h	19.2	43.2	40.9	46.7	25.6	87.9	84.7	85.7
Average (%)			43.6				86.1	

The experiments were performed in triplicate with a fresh PDMS–TiO_2 photocatalytic composite named meso and micro I, II, and III. For the control tests the average values of the triplicate are indicated.

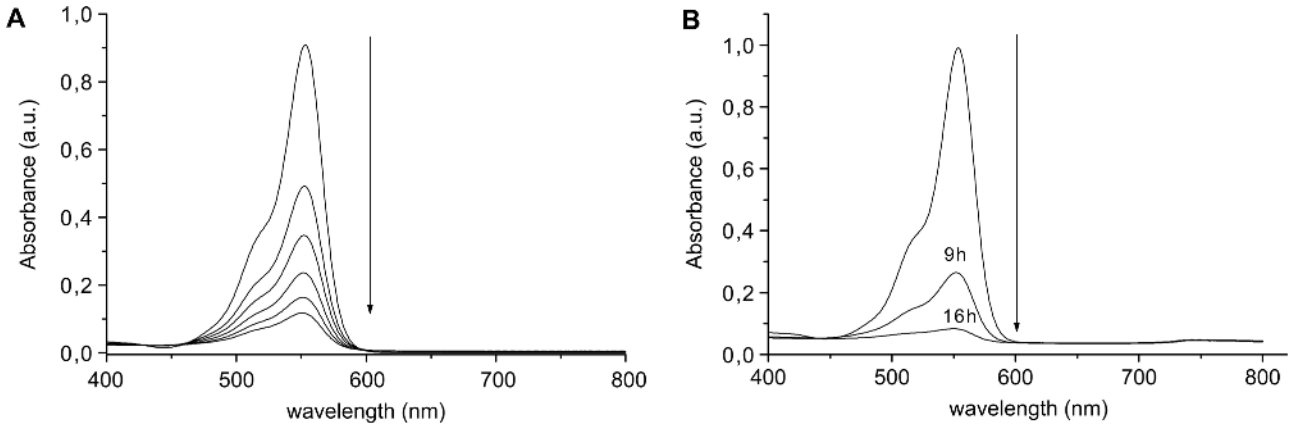

Figure 6. Rhodamine B UV–vis absorbance spectra during: A) 5 flow injection cycles with microreactor syringe pump system; B) continuous flow with microreactor peristaltic pump system

determine the reaction rate constant (k) from the percentage of degradation in micro- and mesoreactor and to compare the performance of the two devices:

$$k = \frac{-\ln(C_x/C_0)}{t} \quad (7)$$

where k represents the reaction rate constant, C_x/C_0 is the degradation of rhodamine B, and t is the effective reaction time [44]. For both photocatalytic reactors, the linearized Eq. (7) is plotted and the rate constant is calculated (Figure 8). For the microreactor, the reaction rate constant was 0.0021/min, while for mesoreactor, k value was 0.0007/min.

All the results previously published have considered only the photodegradation of methylene blue probably because MB is more stable with respect to the rhodamine under UV light and TiO_2 photocatalyst. In our experience, a methylene blue solution 2.7×10^{-5} mol/L was totally degraded in 2 h, while a 10^{-4} mol/L methylene blue solution, in only 3 h. To the best of our knowledge, this is the first study comparing the efficiency of photodegradation of rhodamine B with micro and meso flow reactor. In Table 3, the most significant data reported in the literature have been summarized to compare different experiments of photodegradation of methylene blue in continuous flow and the photodegradation of rhodamine in batch reactor, all of them in presence of TiO_2 under UV irradiation. To the best of our knowledge, this is the first study of photodegradation of rhodamine B with micro and meso flow reactor.

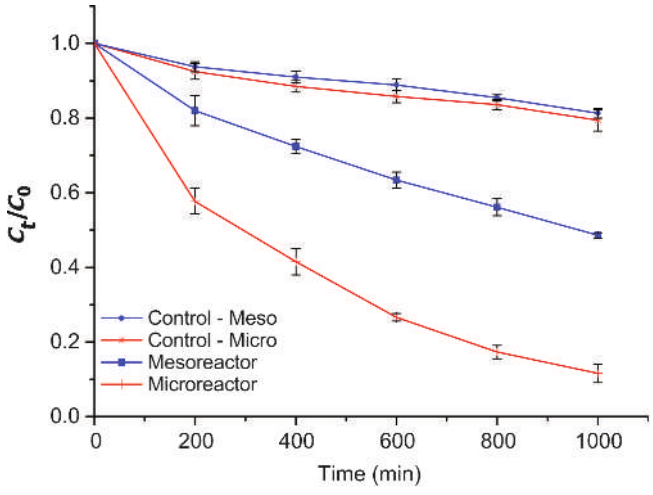

Figure 7. Variation in the rhodamine B concentration in meso- and microreactor syringe pump system after 5 cycles at 0.05 mL/min, with and without a photocatalyst, under UV light irradiation at 12.5 mW/cm^2. The values are an average of triplicate experiments. The bars represent standard deviations

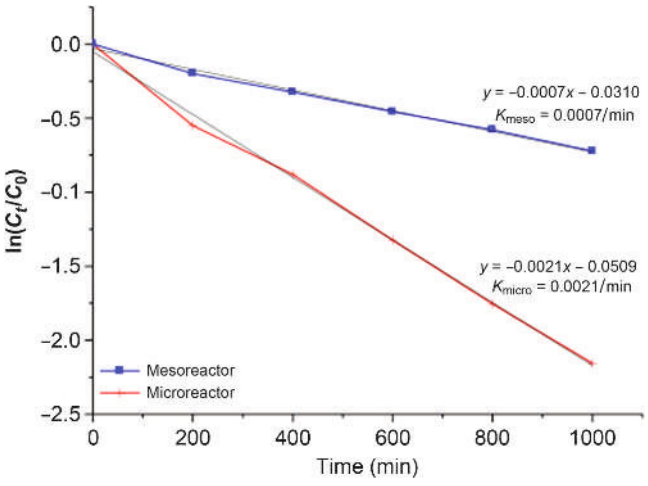

Figure 8. $\ln(C_t/C_0)$ versus the irradiation time, illustrating the reaction rate constant (k) for meso- and microreactors

Table 3. Some of the photocatalytic flow reactor and batch reactor reported in the literature, with respective initial concentration of methylene blue (C0), light source, relative percentage degradation (*D*%), and kinetic constant of the photocatalytic reaction

Photocatalyst	Contact area	C0 (mol/L)	Volume	Flow rate (μL/min)	UV irradiance intensity (mW/cm^2)	*D*%	*k* (/min)	Ref.
Photodegradation of methylene blue in flow								
TiO_2 nanotube anodized on glass	$4.5/cm^2$	1.8×10^{-4}	5 mL	25–100	100	82–92	0.22	52
TiO_2 coated on fiber glass	$3.0/cm^2$	3.1×10^{-5}	24 μL	25–100	50	55–95	4–5	44
ZnO nanowire hydrothermally grown on glass	$9/cm^2$	3.0×10^{-5}	3 mL	150–900	100	48–94	1.6–2.2	53
TiO_2 nanofibrous electrospun on glass	–	–	–	25–100	–	60	4.1–5.2	42
P25 embebbed on PDMS	$2/cm^2$	6.0×10^{-5}	1 μL	–	60	100	0.94	50
P25 drop casted on PDMS	$1.3/cm^2$	1.0×10^{-5}	4 mL	33–66	6 W	55-65	–	40
Photodegradation of rhodamine in batch								
P25 1 g/L	Batch 125 mL	2.1×10^{-5}	2 mL	Batch	5 UV-LED 12 mW/cm^2	96%	–	48
TiO_2-coated on wall reactor	Batch 11 i.d. ×25 cm	4.2×10^{-5}	500 mL	Batch	125 W	95%	–	47
P25 1 g/L	Batch 5.7 i.d. ×16 cm	3.1×10^{-5}	–	Batch	125 W	98%	0.0146	46

3. Conclusions

The integration of a photocatalyst in PDMS for the construction of meso- and microfluidic devices was performed through a low cost and environmentally sustainable method. SEM, EDS, and confocal Raman spectroscopy confirmed the impregnation of TiO_2 in PDMS. The TiO_2 film showed good adhesion to the surface of the PDMS, though some areas were not completely coated. While it is still necessary to improve the deposition technique, the current technique enabled the development of meso- and microfluidic devices with high photocatalytic activity. Microreactor is more efficient than mesoreactor, showing higher photodegradation activity at lower powered UV light. These results highlighted two important factors: the influence of the experimental setup, such as the photocatalytic surface to internal volume of reactor ratio, and the intensity of the irradiation light. The 0.013-mL internal volume of microreactor, compared to the 0.8 mL of the mesoreactor, is ≈62 times smaller, thus, enabling a higher photocatalytic efficiency of the microreactor with lower intensity of UV light. Although the flow injection systems have not revealed significant differences, the semicontinuous flow was useful to determine the reaction rate constant (*k*) of each flow cell, showing the higher performance of microreactor with respect to mesoreactor. Under UV light irradiation of 12.5 mW/cm^2 and with a continuous flow of 0.05 mL/min for 16 h with a peristaltic pump, for meso- and microreactor, a considerable photodegradation of rhodamine B, 43.6% and 86.1%, respectively, was shown. A semicontinuous-flow injection into photocatalytic microreactor by syringe pump system, under UV light irradiation at 12.5 mW/cm^2, showed 88.4% of degradation of rhodamine B, resulting in a performance of 37% higher than for a mesoreactor system. The easy and fast prototyping process together with the small quantity of material used for the photodegradation tests can provide relevant advantages with respect to batch tests. For a scientific viewpoint, a microreactor is very useful for testing small and expensive homemade photocatalyst or other kind of catalyst [54]. For small industrial scale applications, the mesoreactor could overcome some disadvantages of the PDMS microreactor. It can be useful for studying of photodegradation processes with high flow rate with the presence of organic solvents. Further studies will be focused on selective oxidative reactions inside micro- and mesofluidic photocatalytic devices through monitoring the products online.

4. Experimental Section

4.1. Materials and Equipment. All the chemical reagents were used without further purification: P25 titania nanoparticles (TiO_2) from Degussa AG, rhodamine B dye from Sigma-Aldrich, Milli-Q water (18.2 MΩ/cm) from Millipore, absolute ethanol from VETEC, and polymerizing agent Sylgard™ 184 silicone Elastomer KIT for PDMS polymer from Dow Corning Corporation. For the assembling of a flow system injection of rhodamine solution in meso- and microfluidic devices, the following components were used: a syringe pump from Future Chemistry Inc., a peristaltic pump from Syrris Inc., polypropylene pipes for intravenous infusion of 1 mm of diameter, steel needles, Up-church connectors with luer adapter, and a 10-mL plastic lock-luer syringe.

A photocatalytic system consisting of a LED of 365 nm (THORLABS) powered by 100 mW/cm^2 (25 mW/cm^2 at 3.1 cm distance) and a convergent lens to allow the focus of the light beam only in the circular area of the photocatalytic composite materials (diameter of 1.3 cm) was used.

Confocal Raman microscope from Horiba Scientific/Jobin Yvon and field emission scanning electron microscope (FEG-SEM) from JEOL were used to characterize the impregnation of the P25 into PDMS. A spectrometer UV–vis Perkin Elmer Lambda Model 956 was used to evaluate the degradation of rhodamine B solution (10^{-5} mol/L) during the photolysis and photocatalysis experiments.

For microreactor prototyping, to cut a tape (3M Scotch Magic®) glued on microscope glass slide, a laser printer CO_2 (V.30 Laser Desktop, Universal Laser System Inc) was used. Air Cleaner O_2 Plasma from Plasma Harrick was used to hydroxylate the PDMS surfaces and seal the PDMS microreactor.

For mesoreactor prototyping, a Corning Glass Microscope Slide (dimensions 25 × 70 × 1 mm) with no UV absorption and reflection between 250 and 350 nm and a homemade flow cell in polyetheretherketone (PEEK) with a steel holed support as illustrated in AutoCAD and Solid Work designs in Figures S1 and S2, were used.

4.2. Prototyping of Meso- and Microreactor with Photocatalytic TiO_2–PDMS Composite. The common process for the production of photocatalytic TiO_2–PDMS composites is shown in Figure 9 (α–δ). A glass microscope slide was treated with a diamond cutter to create a hole with circular area of 13 mm diameter and 125 μm depth. The glass slide with the empty circular area (Ø = 13 mm, *h* = 125 μm) was used to be filled with TiO_2 powder and was previously fixed in a square box of dimensions 8.7 cm × 8.7 cm × 2.8 cm. A suspension of TiO_2 (P25) 1% w/v in ethanol followed by stirring in ultrasound bath for 10 min was used to deposit P25 to the circular hole of the glass slide. The deposition was conducted in two steps: for each one, 50 μL of the suspension was drop casted, and then, the solvent was evaporated into the oven at 60 °C for 10 min (Figure 9α).

PDMS monomer and a polymerizing agent (Sylgard 184 Silicone Elastomer Kit™) were manually mixed (10:1 ratio) and degassed for 20 min under reduced pressure. The mixture was poured onto the surface glass slide containing a powder

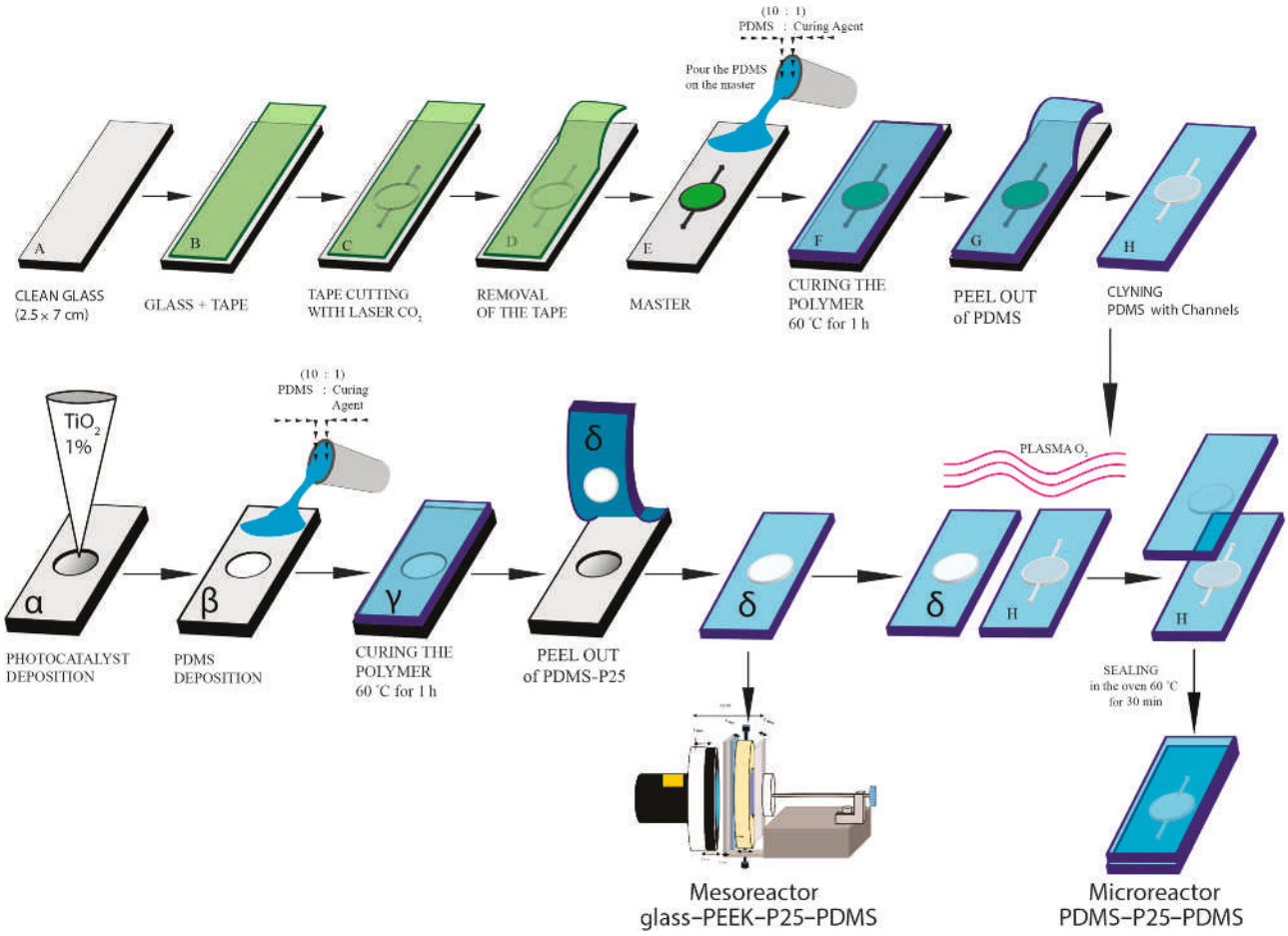

Figure 9. Illustration scheme for rapid prototyping process of microreactors PDMS–TiO_2–PDMS and mesoreactor glass–PEEK–TiO_2–PDMS: (A) cleaning of glass microscope slide; (B) casting of 4 layers of tape on the glass with a total of 200 μm height; (C) cutting of the tape with laser CO_2; (D) removing of the tape to obtain the positive master mold of glass plus tapes; (E) pouring of the degassed mixture of PDMS and polymerizing agent (10:1) on the master mold; (F) curing of the polymer at 60 °C for 1 h; (G) peeling out of negative stamp of PDMS with microchannels and circular area of 200 μm depth; (H) cleaning of PDMS stamp with microchannels; (α) deposition of TiO_2 (1% w/v) on the glass slide with the empty hole area of 125 μm depth; (β) pouring of degassed mixture of PDMS and polymerizing agent (10:1) on the mold with powder layer of TiO_2; (γ) curing of the polymer at 60 °C for 1 h; (δ) peel out of TiO_2–PDMS composite. Finally, the photocatalytic TiO_2–PDMS composite can be screwed against a steel holed support system with a PEEK flow cell and a clean glass slide for the creation of the mesoreactor glass–PEEK–TiO_2–PDMS, or can be sealed with a PDMS stamp (H) under O_2 plasma for the creation of microreactor PDMS–TiO_2–PDMS

layer of P25 deposited on it. It was then taken to an oven at 60 °C for 1 h until the complete curing of the elastomer polymer (Figure 9β–γ). Thereafter, TiO_2–PDMS composite was cut with a scalpel land and peeled out for the further characterization. The photocatalytic composite layer with a circular protrusion of ≈124 μm height was used to build-up both meso- and microreactor devices (Figure 9δ).

Basically, the mesoreactor, shown in Figures 9 and S1 with all the details with AutoCAD design, is built on homemade steel holed support aligning and screwing in sequence: a clean glass microscope slide, a PEEK flow cell with two rubber rings to avoid leak of solution, and the photocatalyst TiO_2–PDMS composite. The PEEK flow cell, with 13-mm hole diameter, 6 mm depth, and 0.8 mL volume capacity, let the UV light pass through the hole directly to the photocatalytic layer located at the bottom of the flow cell reactor system. In the same system, it is possible to replace a TiO_2–PDMS composite with another clean glass microscope slide and use it as a "control" system to study the photolysis phenomena associated only at the light degradation of the organic dye.

The microreactor PDMS–TiO_2–PDMS shown in Figures 9 and S3 was made sealing two PDMS layers by means of O_2 plasma treatment: a PDMS stamp (Figure 9H) with inlet/outlet microchannels and a circular hole of 200 μm depth and the photocatalytic TiO_2–PDMS composite with a circular protrusion of 124 μm height (Figure 9δ). In this configuration, the internal volume is ≈0.013 mL and the depth's chamber is 76 μm. Previously, the TiO_2–PDMS composite was carefully cleaned with ethanol using a swab. The PDMS stamp was cleaned with 5% neutral detergent, rinsed with ultrapure water, and, finally, dried at 60 °C for 1 h after 10 min of ultrasound ethanol bath. Subsequently, the two PDMS models were treated with O_2 plasma for 3 min to promote hydroxylation of the surfaces. The PDMS surfaces, activated by means of the formation of Si–OH groups, were superimposed and sealed. The microreactor PDMS–TiO_2–PDMS was subsequently placed in an oven at 60 °C for 30 min to complete the process of condensation between Si–OH groups. The prototyping of the microreactor PDMS/PDMS system, named "control," follows the same procedure without the drop casting deposition of TiO_2. This microfluidic devise is used as a "control" system to study the photolysis phenomena associated only with the degradation of the organic dye by the action of light. In Figure S4, depicted are the flow reactor systems, meso- or microfluidic devices, both connected to peristaltic and syringe pump system under UV LED light irradiation.

4.3. Characterization of PDMS–TiO_2 Composite. Raman spectra of PDMS–TiO_2 composite were obtained using a confocal Raman microscope (Horiba Scientific/Jobin Yvon), and all data were processed and analyzed by LabSpectra 6 software

Spectroscopy Suite. The sample was excited with an Ar–Kr laser source (wavelengths of 785 nm), objective lens of 100, grating of 1200 g/mm, and filter of 25%. The laser power on the sample was 22.5 mW. 2D and 3D Raman mapping were recorded using a motorized table that gets a Raman spectra each 5 μm step along 20 × 20 μm and 10 μm depth. Each spectrum was acquired with two accumulations for 2 s each. Chemical colored images were generated using defined spectral regions in the acquired spectrum.

A field emission scanning electron microscope (FEG-SEM) (JEOL, JSM-6701 F) was operated in the secondary electron mode at 1 kV with a work distance of 6.0 mm using the LEI detector. The formation of the thin TiO_2 layer on PDMS was verified by energy dispersive X-ray spectroscopy (EDS) operating at 15 kV with a work distance of 15 mm. For SEM morphological characterization, a cross section of PDMS–TiO_2 composite was cut with bistoury and placed on the sample holder with the traversal cross section perpendicular to the electron beam.

The photocatalytic activity of TiO_2–PDMS composite into meso- and microfluidic devices was investigated by injecting an aqueous solution of rhodamine B (10^{-5} mol/L) under 365 nm UV light irradiation powered at 25 and 12.5 mW/cm^2 at 0.05 mL/min flow rate: in continuous flow with peristaltic pump for 16 h or with 5 cycles flow injection by syringe pump (3.3 h each). The absorbance spectra of rhodamine B solution were measured with PerkinElmer Lambda 956 spectrophotometer in the light wavelengths range between 400 and 800 nm. The residual concentration of rhodamine B was monitored observing the decrease of the optical absorbance peak intensity at 553 nm.

4.4. Photocatalytic Activity Test. The experimental setup is depicted in Figures 10 and S4 in the supporting information. All the results are shown in Tables **1** and **2**, and all the experiments, both with micro- and mesofluidic reactors, were performed in triplicate with a fresh PDMS–TiO_2 photocatalytic composite named meso and micro I, II, and III. The photocatalytic tests were carried out with two-flow injection systems: a syringe pump system for a semicontinuous injection and a peristaltic pump system for a continuous injection of the organic dye solution (Figure **10**A and B).

The photodegradation reaction with a syringe pump was performed recycling 5 times 10 mL rhodamine B solution for a total of 16 h, and the UV–vis analysis was followed after each cycle. On the other hand, with a peristaltic pump system, 10 mL rhodamine B solution was continuously cycling during 16 h (loop system), and the UV–vis analysis was performed only at the end of the experiment. The semicontinuous-flow system was useful to understand the photodegradation of rhodamine B at each step without mixing the products generated along the photocatalytic process. On the other hand, it was useful to understand if the continuous-flow process can have better performance compared with the semicontinuous-flow system. Tubing, connectors, luer-lock plastic syringe of 10 mL, and LED system with 365 nm UV light with two irradiation powers of 25 mW/cm^2 and 12.5 mW/cm^2, 10 mL of rhodamine B solution (10^{-5} mol/L), flow rate at 0.05 mL/min, and exposition time were kept constant to compare the performance of the meso- and microfluidic photocatalytic systems.

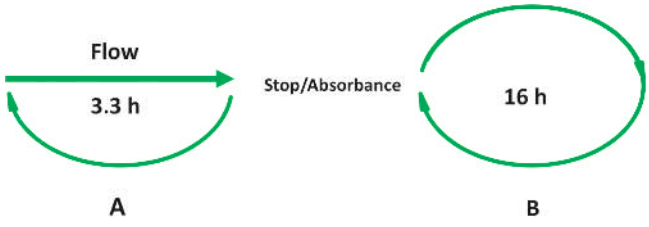

Figure 10. Flow injection setup: A) semicontinuous syringe pump system recycling 5 times 10 mL rhodamine solution for a total of 16 h; B) continuous peristaltic pump system for a constant recycling of the organic dye solution (loop system for 16 h)

Acknowledgment. We gratefully acknowledge the FAPERJ (E-26/112.096/2012) for funding the research and the fellowship of D. S. de Sá (Bolsista FAPERJ nota 10). B. A. M. is grateful to CNPq (National Council for Scientific and Technological Development) for a research productivity grant. We thank João Lucas Rangel of University of Valley of Paraiba for his kind help in confocal Raman spectroscopy and data analysis (2D and 3D image). In addition, we thank Horiba Jobin Yvon for excellent technical support with XploRA system and FCS controles for the manufacturing of the PEEK mesoreactor.

Supporting Information

Electronic Supplementary Material (ESM) containing supplementary data (AutoCAD and solid work design of mesoreactor, flow reactor systems, estimation of velocity and reynolds number (Re) for micro- and mesoreactor) associated with this article can be found in the online version at doi: 10.1556/1846.2015.00043.

References

1. Roberge, D. M.; Gottsponer, M.; Eyholzer, M.; Kockmann, N. *Chim. Oggi* **2009**, *27*, 8–11.
2. Roberge, D. M.; Zimmermann, B.; Rainone, F.; Gottsponer, M.; Eyholzer, M.; Kockmann, N. *Org. Process Res. Dev.*, **2008**, *12*, 905–910.
3. Hartman, R. L.; McMullen, J. P.; Jensen, K. F. *Angew. Chem., Int. Ed.* **2011**, *50*, 7502–7519.
4. Jas, G.; Kirschning, A. *Chem. – A Eur. J.* **2003**, *9*, 5708–5723.
5. Wegner, J.; Ceylan, S.; Kirschning, A. *Chem. Commun.* **2011**, *47*, 4583–4592.
6. Souza, R. O. M. A. de; Miranda, L. S. M. *Rev. Virtual Quím.* **2014**, *6*, 34–43.
7. Falk, L.; Commenge, J.-M. *Chem. Eng. Sci.* **2010**, *65*, 405–411.
8. Mehendale, S. S.; Jacobi, A. M.; Shah, R. K. *Appl. Mech. Rev.* **2000**, *53*, 175–193.
9. Elvira, K. S.; Casadevall i Solvas, X.; Wootton, R. C. R.; DeMello, A. J. *Nat. Chem.* **2013**, *5*, 905–915.
10. Yao, X.; Zhang, Y.; Du, L.; Liu, J.; Yao, J. *Renewable Sustainable Energy Rev.* **2015**, *47*, 519–539.
11. Mehendale, S. S.; Jacobi, A. M.; Shah, R. K. In *Heat and Mass Transfer*; Lehner, M.; Mewes, D., Eds.; Springer Berlin/Heidelberg, 1999; Part I, pp. 139–158.
12. Zheng, M.; Skelton, R. L.; Mackley, M. R. *Process Saf. Environ. Prot.* **2007**, *85*, 365–371.
13. McMullen, J. P.; Stone, M. T.; Buchwald, S. L.; Jensen, K. F. *Angew. Chem., Int. Ed.* **2010**, *49*, 7076–7080.
14. Mark, D.; Haeberle, S.; Roth, G.; von Stetten, F.; Zengerle. R. *Chem. Soc. Rev.* **2010**, *39*, 1153–1182.
15. Vandermeersch, T.; Goovaerts, R.; Luyten, J.; Denayer, J. F. M.; De Malsche, W. *Chem. Eng. J.* **2015**, *279*, 9–17.
16. Rivet, C.; Lee, H.; Hirsch, A.; Hamilton, S.; Lu, H. *Chem. Eng. Sci.* **2011**, *66*, 1490–1507.
17. Nieto, D.; Couceiro, R.; Aymerich, M.; Lopez-Lopez, R.; Abal, M.; Flores-Arias, M. T. *Colloids Surf. B* **2015**, *134*, 363–369.
18. Pandoli, O.; Del Rosso, T.; Aucélio, R. Q.; Massi, A.; Xiang, C.; Hysing, S.-R. *J. Flow Chem.* **2014**, *4*, 61–65.
19. Wang, N.; Zhang, X.; Wang, Y.; Yu, W.; Chan, H. L. W. *Lab. Chip* **2014**, *14*, 1074–1082.
20. Valera, F. E.; Quaranta, M.; Moran, A.; Blacker, J.; Armstrong, A.; Cabral, J. T.; Blackmond, D. G. *Angew. Chem., Int. Ed.* **2010**, *49*, 2478–2485.
21. Hessel, V.; Cortese, B.; de Croon, M. H. J. M. *Chem. Eng. Sci.* **2011**, *66*, 1426–1448.
22. Ren, K.; Zhou, J.; Wu, H. *Accounts Chemical Research* **2013**, *46*, 2396-2406.
23. Kotowski, J.; Šnita, D. *Microelectron. Eng.* **2014**, *125*, 83–88.
24. Pimparkar, K.; Yen, B.; Goodellm J. R.; Martin, V. I.; Lee, W.-H.; Porco, J. A.; Beeler, A. B.; Jensen, K. F. *J. Flow Chem.* **2011**, *1*, 53–55.
25. Sollier, E.; Murray, C.; Maoddi, P.; Di Carlo, D. *Lab. Chip* **2011**, *11*, 3752–3765.
26. Whitesides, G. M. *Nature* **2006**, *442*, 368–373.
27. Zhou, J.; Ellis, A. V.; Voelcker, N. H. *Electrophoresis* **2010**, *31*, 2–16.
28. Paul, D. R.; Mark, J. E. *Prog. Polym. Sci.* **2010**, *35*, 893–901.
29. Na-Meng; Zhou, N.-L. *Appl. Clay Sci.* **2012**, *70*, 22–27.
30. Li, X.; Wu, N.; Rojanasakul, Y.; Liu, Y. *Sens. Actuators. A* **2013**, *193*, 186–192.
31. Kim, M. "Mike"; Huang, Y.; Choi, K.; Hidrovo, C. H. *Microelectron. Eng.* **2014**, *124*, 66–75.
32. Lee, J. N.; Park, C.; Whitesides, G. M. *Analytical Chemistry* **2003**, *75*, 6544–6554.
33. Izadifard, M.; Achari, G.; Langford, C. H. *Catalyst* **2013**, *3*, 726–743.

34. Védrine, J. C. *Appl. Catal., A* **2014**, *474*, 40–50
35. Tavares, M. T. S.; Santos, A. S. F.; Santos, I. M. G.; Silva, M. R. S.; Bomio, M. R. D.; Longo, E.; Paskocimas, C. A.; Motta, F. V. *Surf. Coat. Technol.* **2014**, *239*, 16–19.
36. Deng, Z.-Y.; Wang, W.; Mao, L.-H.; Wang, C.-F.; Chen, S. *J. Mater. Chem. A* **2014**, *2*, 4178-4184.
37. Li, M.; Deng, T.; Liu, S.; Zhang, F.; Zhang, G. *Appl. Surf. Sci.* **2014**, *297*, 147–152.
38. Lee, S.-Y.; Park, S.-J. *J. Ind. Eng. Chem.* **2013**, *19*, 1761–1769.
39. Hernández-Alonso, M. D.; Fresno, F.; Suárez, S.; Coronado, J. M. *Energy Environ. Sci.* **2009**, *2*, 1231-1257.
40. Pandoli, O.; Rosso, T. D.; Santos, V. M.; de Rezende, R. S.; Marinkovic, B. A. *Quim. Nova* **2015**, *38*, 859–863.
41. Castellana, E. T.; Kataoka, S.; Albertorio, F.; Cremer, P. S. **2005**, *78*, 1275–1280.
42. Meng, Z.; Zhang, X.; Qin, J. *Nanoscale* **2013**, *5*, 4687-4690.
43. Lei, L.; Wang, N.; Zhang, X. M.; Tai, Q.; Tsai, D. P.; Chan, H. L. W. *Biomicrofluidics* **2010**, *4*, 43004–43016.
44. Li, L.; Chen, R.; Zhu, X.; Wang, H.; Wang, Y.; Liao, Q.; Wang, D. *ACS Appl. Mater. Interfaces* **2013**, *5*, 12548–12553.
45. Wang, N.; Lei, L.; Zhang, X. M.; Tsang, Y. H.; Chen, Y.; Chan, H. L. W. *Microelectron. Eng.* **2011**, *88*, 2797–2799.
46. Aarthi, T.; Madras, G. *Ind. Eng. Chem. Res.* **2007**, *46*, 7–14.
47. Barka, N.; Qourzal, S.; Assabbane, A.; Nounah, A.; Ait-Ichou, Y. J. *Photochem. Photobiol. A Chem.* **2008**, *195*, 346–351.
48. Natarajan, T. S.; Thomas, M.; Natarajan, K.; Bajaj, H. C.; Tayade, R. J. *Chem. Eng. J.* **2011**, *169*, 126–134.
49. Sauer, T.; Cesconeto Neto, G.; José, H.; Moreira, R. F. P. *J. Photochem. Photobiol. A Chem.* **2002**, *149*, 147–154.
50. Lamberti, A. *Appl. Surf. Sci.* **2015**, *335*, 50–54.
51. Qin, X.; Jing, L.; Tian, G.; Qu, Y.; Feng, Y. *J. Hazard. Mater.* **2009**, *172*, 1168–1174.
52. Jayamohan, H.; Smith, Y. R.; Hansen, L. C.; Mohanty, S. K.; Gale, B. K.; Misra, M. *Appl. Catal. B Environ.* **2015**, *174–175*, 167–175.
53. Han, Z.; Li, J.; He, W.; Li, S.; Li, Z.; Chu, J.; Chen, Y. *Microelectron. Eng.* **2013**, *111*, 199–203.
54. Zhang, H.; Wang, J.-J.; Fan, J.; Fang, Q. *Talanta* **2013**, *116*, 946–950.